Rapid on-chip integration of opal films and photonic gel sensor array via directed enhanced water evaporation for colloidal assembly

Seungjae Lee [a],[1], Young-Lo Lee [b],[1], Bomin Kim [a], Kunhyuk Kwon [a], Joohyun Park [a], Kyusung Han [c], Hyunjung Lee [d], Wonmok Lee [a],*

[a] Department of Chemistry, Sejong University, 98 Gunja-dong, Gwangjin-gu, Seoul 143-747, Republic of Korea
[b] Department of Chemistry, Sogang University, 35 Baekbeom-ro, Mapo-gu, Seoul 04107, Republic of Korea
[c] Korea Institute of Ceramic Engineering and Technology, Icheon, Gyeonggi 467-843, Republic of Korea
[d] School of Advanced Materials Engineering, Kookmin University, 861-1 Jeongneung-dong, Seoul 136-702, Republic of Korea

ARTICLE INFO

ABSTRACT

We developed a fabrication method for colloidal photonic crystal films and arrays with high quality and uniform thickness without need for any lithography. The method, "directed enhanced evaporation for colloidal assembly" (DEECA), employs a two-step process: a capillarity-induced infilling of an aqueous dispersion of colloidal particles within the thin two-dimensional (2D) channel arrays, followed by enhanced evaporation of water through the inlet, leading to laminar flow of the colloidal dispersion and subsequent colloidal crystallization. DEECA was confirmed to be a fast, precise and a cost-effective process with minimum loss of colloidal particles for preparing multiple opalline scaffold structures toward on-chip integrated photonic bandgap device arrays. To prove this, 2D arrays of poly(hydroxyethylmethacrylate) (PHEMA)-based inverse opal (IO) photonic gel pH sensors were fabricated via templated-photopolymerization of the precursor mixtures within the DEECA cells. It was confirmed that on-chip integrated photonic gel pH sensor arrays could be successfully implemented by using opal templates prepared via DEECA. DEECA could also be utilized for opal-templated fabrication of TiO_2 inorganic IO film arrays on a glass substrate.

© 2016 Elsevier B.V. All rights reserved.

1. Introduction

For the past decade, two-dimensional (2D) and three-dimensional (3D) close-packed structures of submicron-sized colloidal particles have been extensively studied since they are useful scaffold structures for various photonic crystal devices, such as photonic gel sensors [1–6], reflective displays [7], solar cells [8–10], and others [11–13]. Three-dimensional close-packed colloidal crystals, which are also known as synthetic opals, can be fabricated by spin coating [14], vertical deposition [15,16], and direct coating [17,18] from charge stabilized colloidal suspensions in aqueous media. The driving force of the close-packed structure of synthetic opal is primarily based on the capillarity of evaporating water [19]. When a synthetic opal is fabricated via the capillary force of drying solvent, the colloidal crystal film produced usually possesses a face centered cubic (FCC) {111} facet parallel to

the glass substrate, which has the least surface energy compared to other facets. Such {111}-faceted colloidal crystals can be effectively utilized as templates for highly reflective photonic crystals. The synthetic opal film can either be formed on a flat substrate or in between two glass plates. As an example of the former, fabrication of colloidal crystal films was demonstrated by spin-coating a concentrated colloidal dispersion in liquid mixtures with varying composition [14]. Depending on the spin rate and solvent composition, large-area colloidal crystals were obtained with controlled crystalline orientations and film thicknesses. Jiang et al., reported that controlled drying of a colloidal suspension enables vertical coating of a high-quality opalline colloidal crystal on a glass substrate [16]. The method has been improved by Vlasov et al., by applying thermal agitation of the suspension to prevent sedimentation of the colloidal particles during vertical coating [15]. Park and coworkers reported a rapid fabrication of colloidal crystal films by vertical coating of a colloidal suspension via solvent evaporation aided by nitrogen flow [20,21]. However, the vertical coating methods produce a large amount of wasted colloidal dispersion after the coating process. Recently, we presented a horizontal coating process with continuous addition of colloidal suspension, which

* Corresponding author. Fax: +82 2 3408 3212.
E-mail addresses: wonmoklee@sejong.ac.kr, wonmoklee@gmail.com (W. Lee).
[1] These two authors contributed equally to this work.

exhibits rapid colloidal crystallization without significant loss of the colloidal suspension [18]. A simple design of the coating device enabled rapid fabrication of a large-area colloidal crystal (2×2 cm^2) within 20 min, and the colloidal crystal film could also be coated on a flexible polymer film by preparing a colloidal dispersion in an alcoholic medium [22]. A major drawback of the coating methods mentioned thus far is that it is difficult to obtain a uniform opal film with a predefined thickness, and therefore the infilling of functional materials within the opal template can be tricky. An opal film with a desired thickness can be fabricated by crystallizing the colloidal dispersion within a thin 2D channel. Park et al., have developed a method to fabricate large-area opal films with a defined thickness and area by flowing an aqueous colloidal dispersion within a rectangular space while water is drained through a lithographically defined thin channel [23]. An opal film within a flow cell can be appropriately used as a scaffold structure for the subsequent formation of functional devices such as inverse opal (IO) hydrogel sensors. However, the fabrication time to obtain a 1 cm^2 opal film was several weeks because of the slow drainage of water through the thin channel. Miguez et al., developed a method called assisted directed evaporation-induced self-assembly (ADEISA), where the exact addressing of a colloidal crystal within a very thin channel was demonstrated toward sophisticated photonic bandgap devices [24]. In this study, we demonstrate a simple and rapid fabrication method for 2D opal film arrays, in which enhanced water evaporation induces rapid colloidal self assembly within individual channels on a single substrate. The usefulness of the opal film arrays was tested by utilizing them as template structures for the fabrication of IO photonic gel sensors.

2. Materials and methods

2.1. Preparation of PS μ-spheres, silica μ-spheres, and TiO$_2$ nanoparticles

Polystyrene (PS) μ-spheres with various particle sizes and narrow size distributions were synthesized by emulsion polymerization as reported elsewhere [25]. After purging temperature-stabilized deionized (DI) water under N$_2$ flow for 1 h, potassium persulfate (Aldrich) as an initiator and sodium dodecylsulfate (SDS, Aldrich) as a surfactant were added, followed by the quick addition of styrene (Aldrich), which had been filtered through activated alumina to remove the inhibitor. After finishing polymerization at 70 °C for 4 h, the as-synthesized polymer dispersion was filtered through pre-cleaned cotton fibers and poured into a semi-permeable cellulose membrane tube (MWCO 12,000–14,000, MFPI). The emulsion-filled tube was fully soaked in a 5-L beaker containing DI water. The low molecular weight impurities in the tube were removed in this manner. Fresh DI water was exchanged every 4 h until the resistivity of the DI water in the beaker reached 10 MΩ. The final aqueous dispersions contained ~10 wt% of polymer μ-spheres. By controlling the amount of SDS in the reaction batch, seven PS μ-spheres with different particle sizes were synthesized. The average particle sizes characterized by scanning electron microscopy were 197 nm (PS 197), 226 nm (PS 226), 228 nm (PS 228), 238 nm (PS 238), 240 nm (PS 240), 260 nm (PS 260), 267 nm (PS 267), and 300 nm (PS 300), respectively. The average particle size and size distribution of the colloidal dispersion were characterized using an electrophoretic light scattering analyzer (ELS 8000, Otsuka electronics Co.). All the μ-spheres showed a size distribution with a standard deviation of 5%.

Silica μ-particles with two different sizes of 245 nm and 268 nm were synthesized by a typical Stober process [26]. First, a mixture A containing 0.8 M of ammonium hydroxide (Aldrich) in DI water and a mixture B containing 0.1 M (or 0.2 M) of tetraethylorthosilicate (TEOS, Aldrich) in ethanol (Aldrich, spectrophotometric grade) were prepared. Mixtures A and B were mixed with a 1:1 volume ratio with vigorous stirring at 30 °C, and the sol–gel reaction proceeded for 3 h. The precipitate was centrifuged at 4000 rpm for about 10 min, and then the sediments were washed with distilled water five times.

Organically modified TiO$_2$ nanoparticles with an average particle size of 2 nm were synthesized by the sol–gel method in the presence of acetylacetone as an organic modifier [27]. A mass of 5.006 g of acetyl acetone (AcAc) (Aldrich) was added to a round bottom flask containing 34.06 g of 1-butanol (Duksan Chemical) with vigorous stirring. Subsequently, 17.018 g of titanium n-butoxide (Aldrich) was slowly added, and then the solution turned bright yellow upon mixing. While maintaining the reactor temperature at 60 °C, 1.9022 g of p-toluene sulfonic acid (Aldrich) dissolved in 9 g of deionized (DI) water was added drop-wise to the precursor solution to conduct the sol–gel reaction for 24 h. The yellow product was precipitated in an excess amount of toluene, and the precipitate was subsequently centrifuged, washed with toluene and vacuum dried.

2.2. Fabrication of the multi-DEECA cell assembly

The cell assembly consisted of three major parts. All of the glass parts were cleaned with Piranha solution (H$_2$SO$_4$:H$_2$O$_2$ = 3:1 by volume) and rinsed with DI water several times prior to use. The bottom substrate was a flat rectangular glass plate (4×5 cm^2). The top glass plate of the same size had drilled holes (diameter = 1 mm) that were placed at the top centers of the individual cells, and it was rendered hydrophobic using 1 mM trichlorooctadecylsilane dissolved in 2,2,4-trimethylpentane (Junsei) for 20 min. In order to provide three thin spaces between two plates, 25-μm-thick Surlin® film was cut into 4.5 cm-long lanes with a width of 0.7 cm and a spacing of 0.3 cm between each lane, which had open ends for infiltration of the emulsion and drying. The Surlin spacer for five lanes was cut to have a width of 0.4 cm and a spacing of 0.3 cm between lanes. Each spacer was cut using a plotter pen (CC330-20, Grahtec) according to a simple bitmap drawing. The cleaned glass parts and a spacer were stacked as shown in Fig. 1(a), with the top glass placed slightly mismatched from the bottom substrate to leave room for colloid injection, and Surlin was hot-bonded to each glass using a hot-press apparatus at 70 °C to form ~20-μm-thick channels.

2.3. Fabrication of IO photonic gel sensor array with different gel compositions

After degassing the colloidal dispersion of PS-228 by ultrasonication in a bath sonicator (SD-80H, Seong Dong), 2.4 μL of PS-228 colloidal dispersion was measured exactly and infiltrated into each channel, as shown in Fig. 1(b), which proceeded rapidly because of the capillary force. After every channel was filled with dispersion, the holes on the top cell were taped so that water evaporation occurred only on the front side of the channel. The evaporation of water induced FCC stacking of colloidal particles, which usually required 2–3 h (Fig. 1(c)). Fully dried PS opal films were annealed at 90 °C in a convection oven (LK-Lab Korea) to form necking between the neighboring particles (Fig. 1(d)). Next, three different monomer mixtures were prepared to be infilled within each opal film. Mixture 1 contained 2.5 g 2-hydroxyethyl methacrylate (HEMA, Junsei), 35 mg acrylic acid (AA, Junsei), 25 mg ethylene glycol dimethacrylate (EGDM, Aldrich), 75 mg Irgacure-651 (Ciba specialty Chemicals), and 0.625 g DI water. Mixture 2 was the same as mixture 1, except that it contained 35 mg of methacrylic acid (MA, Aldrich) instead of AA, and mixture 3 was also the same except for 35 mg of vinylimidazole (VI, Aldrich) instead of AA.

An aliquot of about 1 μL of the each mixture was infiltrated within the opal templates, as shown in Fig. 1(e), and photo-
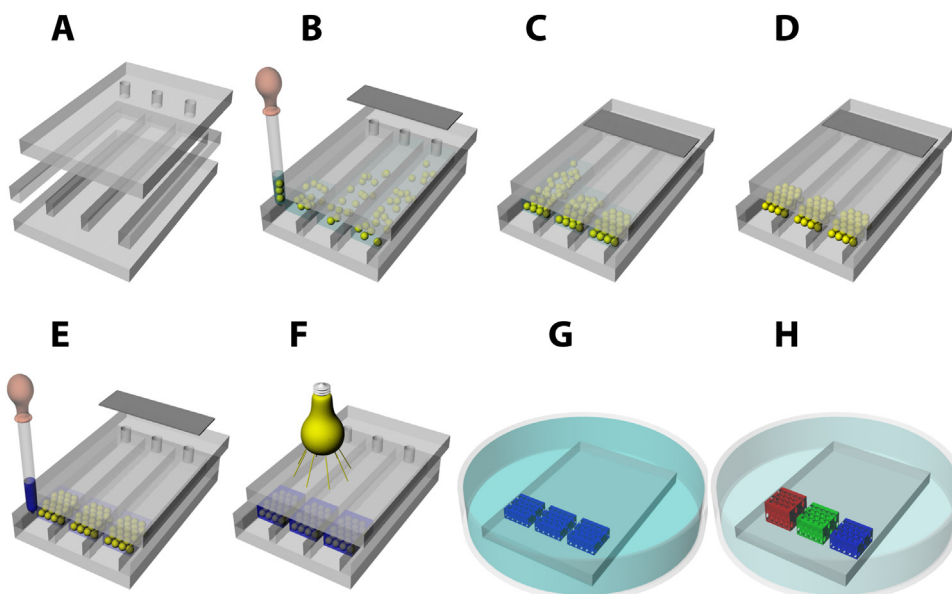
Fig. 1. Schematic diagram of fabrication procedures for the IO sensor array. (a) A top glass plate with drilled holes, a 25-μm-thick Surlin spacer, and a bottom glass plate are assembled and bonded together; (b) a measured amount of aqueous PS dispersion is infiltrated into each of 7×45-mm^2-wide channel, and, once every channel is infilled, the holes on the top plate are closed using silicon tape; (c) colloidal assembly occurs on the front side of each cell because of the capillary force accompanied by drying water flux; (d) dried opal films are annealed at 90 °C; (e) after removing the tape, different monomer mixtures are infiltrated into each cell; (f) photo-polymerization occurs by UV irradiation; (g) after the top plate and the spacer are removed, the opal template is etched away with chloroform; (h) and finally the IO sensor arrays are transferred to the aqueous analyte solution to show different swelling behaviors. (For interpretation of the references to color in this figure legend, the reader is referred to the web version of this article.)

polymerization was performed using a high intensity UV–lamp (SB-100P/F, Spectronics Corporation) through a home-made epoxy filter (Hardex) for 1 h (Fig. 1(f)). Upon completion of photopolymerization of the hydrogel, the top substrate and spacer were removed, and the opal-templated hydrogel was dipped in chloroform (Duksan Pure Chemicals) for 24 h to remove the PS colloidal template (Fig. 1(g)). Subsequent rinsing with chloroform and dipping in acetonitrile (ACN, Duksan Pure Chemicals) produced iridescent color arrays, showing the successful polymerization of IO hydrogel structures. The hydrogel arrays were finally soaked in pH 1.5 phosphate buffer solution via DI water to exhibit different swelling responses, as shown in Fig. 1(h). The phosphate buffer solutions of various pH values were prepared by mixing different volumes of 0.1 M KH$_2$PO$_4$ (aq.) (Duksan Pure Chemicals), 0.1 M HCl (aq.) (Samchun Chemicals), 0.1 M NaOH (aq.) (Samchun Chemicals). pH measurement of the hydrogel sensor was performed using a pH meter (SP-701, Suntex) at room temperature.

2.4. Fabrication of opal film arrays with different colloidal sizes and an IO pH sensor array

To fabricate five opal films with different particle sizes on one plate, five narrow channels (0.4 cm in width) were formed by cutting Surlin film accordingly, and 1-μL aliquots of the degassed PS dispersions (PS-197, PS-226, PS-228, PS-238, and PS-240, ~10 wt%) were infiltrated into each channel. After drying and annealing the opal films, a 1-μL aliquot of Mixtures 1 or 3 was infiltrated within each opal film, and the entire cells were exposed to UV–light for photo-polymerization. The following steps were the same for each of the three sensor arrays.

2.5. Characterization of opal and IO films

To characterize the opal and IO films, high-resolution transmission electron microscopy (HR-TEM, Tecnai F20, FEI), and scanning electron microscopy (SEM, S-4700, Hitachi) were used. The reflec-

tive colors of the IO films were analyzed using a DSLR camera (DSLR-A550, Sony). The reflectance of the films was measured using a fiber optic UV–vis spectrometer (AvaSpec, Avantes) connected to a reflected light microscope (L2003A, Bimeince) through an objective lens (20 × /0.30 NA) as shown in Fig. 1(b). In each measurement, the raw data of the reflected signal from the sample were referenced by a silver mirror (Edmund Optics).

2.6. Calculation of the peak reflectance wavelength for opal and IO films by a modified Bragg equation

Because of the long-range ordering of the colloidal opal structure, the fabricated opal films and IO photonic gel films exhibited structural colors due to Bragg diffraction of room light from the FCC {111} layers, and the peak wavelengths (λ_{peak}) of the diffraction spectra normal to the plane of the opal are related to the particle diameter d as follows.

$$\lambda_{peak} = 1.633 \times d \times (f_{PS \times} n_{PS}{}^2 + f_{air} \times n_{air}{}^2)^{1/2}$$

$$= 1.633 \times d \times n_{eff}$$

where n_{PS}, n_{air}, f_{PS}, and f_{air} are the refractive indices and filling factors of the PS and air, respectively; Typically, n_{eff} of PS opal film is about 1.47, and that of silica opal is ~1.37. For an FCC IO structure of PHEMA hydrogel, one can estimate n_{eff} of hydrogel in water as ~1.38.

3. Results and discussion

3.1. Rapid fabrication of 2D opal film array

Our method is called "directed enhanced evaporation for colloidal assembly" (DEECA), and technically distinguished from ADEISA developed by Ozin and coworkers in which very thin channels were created by a soft lithographic technique. Nonetheless, DEECA is similar to ADEISA in a sense that a colloidal suspen-
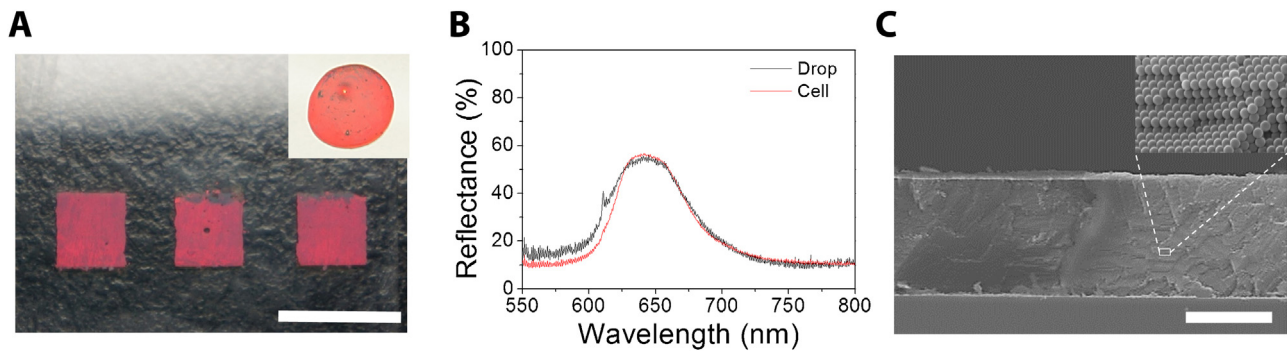
Fig. 2. PS Opal films fabricated by DEECA using PS267. Photograph of an opal film array by DEECA and by drop-cast opal (inset figure) showing red reflective colors, (b) reflectance spectra of drop-cast (black) and DEECA-cast (red) opals showing peak reflectances (λ_{peak}) at 648 nm for both films, and (c) cross-sectional SEM image showing the uniform thickness of a DEECA-cast opal film. The inset shows a magnified view of the designated area. The scale bars in (a) and (c) respectively indicate 1 cm and 10 μm. (For interpretation of the references to color in this figure legend, the reader is referred to the web version of this article.)
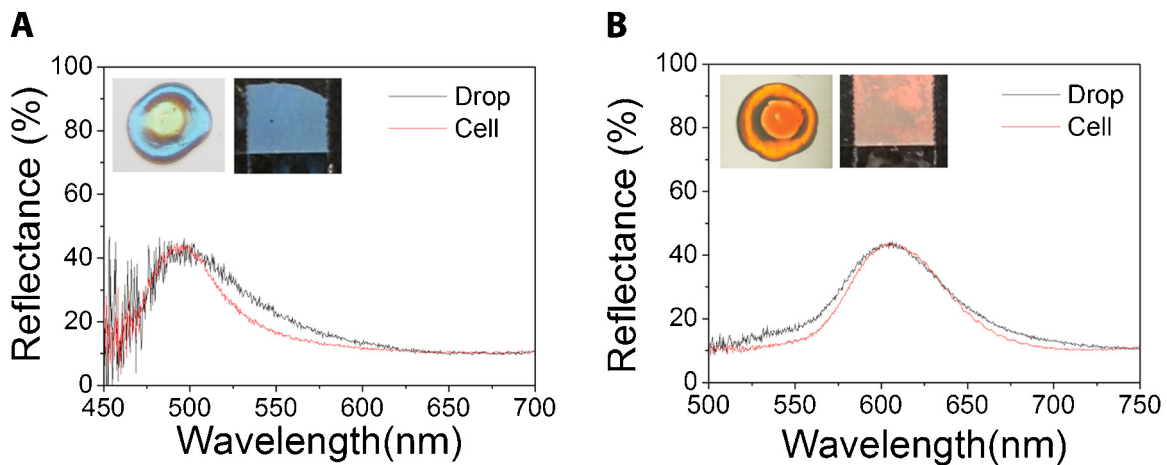

Fig. 3. Reflectance spectra of silica opal films of (a) silica-245, (b) silica-268 fabricated by drop casting (black curve) and DEECA (red curve) respectively. Inset figures in each graph are the photographs of drop-cast film (left) and DEECA-cast film (right). (For interpretation of the references to color in this figure legend, the reader is referred to the web version of this article.)

sion is infiltrated within a channel by capillarity. With DEECA, we aimed to fabricate opal films and arrays with high quality and uniform thickness without any lithographic work, and DEECA can thus provide a cost-effective process to prepare scaffold structures for on-chip integrated photonic bandgap device arrays. The most distinguished feature of DEECA is that different opal films or different IO structures can be on-chip integrated in a simple way. This should be particularly advantageous for the fabrication of diagnostic or environmental sensor arrays. The basic idea is to fabricate 2D arrays of rectangular channels with (1) a wide open end for rapid water evaporation and subsequent capillarity-induced colloidal crystallization, (2) less than 100 μm of thickness to ensure a evaporation-induced laminar flow of the colloidal dispersion, and (3) a small hole drilled at the other side of the channel to facilitate the infiltration of aqueous colloidal dispersions. (Fig. 1(a))

The shape of the channel was determined by the Surlin spacer, which was cut using a plotter pen according to a simple bitmap drawing. No sophisticated computer-aided design (CAD) tool or lithographic tool was employed. Upon loading a calculated amount of dispersion at the open end, each channel was filled by capillary force, the concentrated dispersion began to dry, and the colloidal particles were self-assembled along with evaporating water flux. By capping the drilled holes with an adhesive tape after infilling of a dispersion, evaporation and directed colloidal self-assembly occurred only at the open inlet of the channels. For instance, the

evaporation of a 10 wt% colloidal dispersion within the channel created a ~5 mm × 7 mm opal film formation at the front side of the channel, as shown in Fig. 1(c). Rectangular opal films can be obtained within 1–2 h through DEECA, depending on the particle size, which is substantially faster than the previously reported methods in which particle packing was promoted by external pressure and slow water drainage through a thin channel [1,23]. In addition to rapid colloidal crystallization, a high-quality opal film with uniform thickness could be obtained owing to the uniform laminar flow of the colloidal dispersion within a thin (~20 μm) channel toward the channel end and the accompanying directed assembly of the opal film at the end of the channel [28]. Fig. 2(a) shows the photographs of the opal films fabricated by DEECA using PS267, which corresponds to a fabrication stage in Fig. 1(c). Since the top glass plate surface was rendered hydrophobic, opal films remained on the bottom plate upon disassembly of the glass plates. Shown in inset of Fig. 2(a) is a drop-cast film from the same PS emulsion. As shown in Fig. 2(b), λ_{peak} of PS267 opal film appears to be 648 nm which shows a good coincidence with the estimated value of 641 nm from the modified Bragg equation. Since the red reflective colors of the drop-cast and DEECA-cast opals in Fig. 2(a) are hard to compare, the quality of the opal films was characterized using a reflectance spectrometer, as shown in Fig. 2(b), which revealed that the full width at half maximum (FWHM) of a cell-cast opal was ~20% narrower than that of the drop-cast film. An
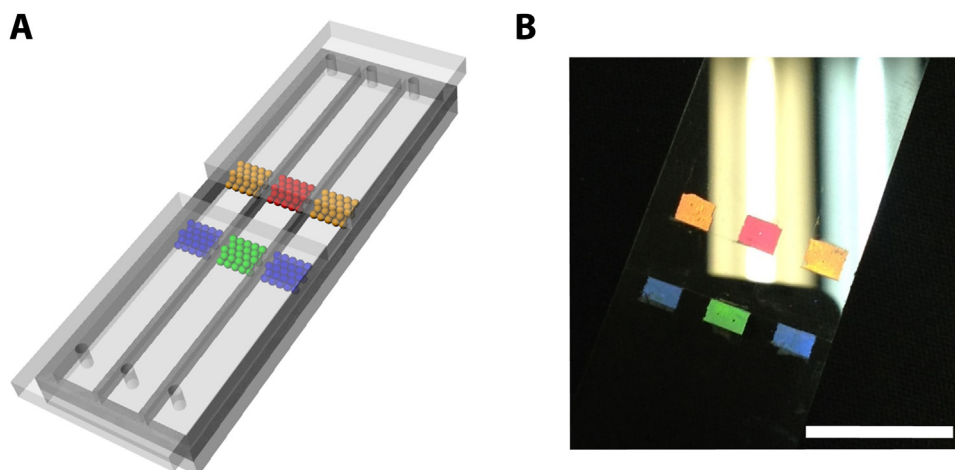
Fig. 4. 2 × 3 opal film arrays of PS197, PS226, PS260, and PS267 fabricated from double-cell arrays. (a) Schematic figure of a double-cell array with six individual opal films cast in six channels and (b) a photograph showing six opal films cast in 2 × 3 cell arrays. Different reflective colors are shown. The scale bar indicates 2 cm. (See Fig. S2 for more pictures). (For interpretation of the references to color in this figure legend, the reader is referred to the web version of this article.)

improved FWHM of a cell-cast opal film implies a better arrangement of the opal array owing to the geometrical constraint effect of the thin channel to direct opal assembly. As shown in Fig. 2(c), the cell-cast opal film also showed uniform thickness corresponding to the 25-μm-thick Surlin film used as a spacer film for the cell. In addition, a large area opal film can be obtained by simply increasing the channel size of DEECA cell without significant loss of film quality (See Fig. S1).

The improved opal quality by DEECA-casting was more obviously manifested in the fabrication of silica opal film by DEECA. Aqueous dispersions of silica particles with different sizes (245 nm vs. 268 nm) were fabricated into opal films by drop casting and cell casting. Fig. 3(a) and (b) are the reflectance spectra of silica-245 and silica-268 respectively in which the inset figures show the ring-shaped drop-cast films and DEECA-cast (rectangular shape) films from the two silica particles. The opal films from silica-245 showed greenish blue reflective colors, while those from silica-268 exhibited orange colors. Just as PS opal films, silica opals by DEECA show narrower reflection peaks than those by simple drop casting due to better crystallinities of DEECA-cast opal films

For a better comparison, the peak reflectances of the DEECA-cast opals were normalized to those of the drop-cast opals in Fig. 3(a) and (b) although they both showed higher reflectances. Like the PS opal fabrication, the silica opals fabricated by DEECA showed narrower reflectance spectra compared to the drop-cast ones, demonstrating that DEECA also resulted in better oriented silica opal films.

The apparatus for DEECA was modified to obtain 2 × 3 on-chip integrated opal film arrays. Fig. 4(a) is a 3D image of 2 × 3 opal film fabrication, in which two top plates were placed on one bottom plate to fabricate three channels of opal films (See Fig. S2 for more images). Since the channels were physically isolated by the spacer film, different colloidal dispersions or different precursor mixtures could easily fill the individual channels. As shown in Fig. 4(b), 2 × 3 individual opal films exhibiting distinct reflective colors could be successfully fabricated by DEECA. Since the major driving forces of high-quality opal formation in DEECA are enhanced water evaporation at the wide open end of the channel and the accompanying laminar flow of the colloidal suspension within the thin channel, it allows diverse 2D arrangements of opal film arrays on rigid or flexible substrates. Such features enable on-chip integration of opal-based photonic bandgap devices by a relatively simple process.

3.2. Photonic gel sensor arrays with different PS particles

As a demonstration of the on-chip integrated photonic device using DEECA, a linear photonic gel sensor array was fabricated. Five PS colloidal dispersions of different particle sizes were infiltrated into a five-cell array, and the dried opal template arrays were filled with the same precursor mixture of VI. In Fig. 5(a), the photographs from top to bottom were taken during infiltration of the five colloidal dispersions, drying of the opal arrays, photo-curing of the infiltrated precursor mixture, etching of colloidal templates in chloroform, immersion of the sensor array in pH 2 buffer, and finally immersion in pH 5 buffer, respectively. To help the reader's understanding, each stage of photonic gel sensor fabrication is schematically drawn in Fig. 5(b).

The resulting IO photonic gel arrays exhibited distinguishable reflective colors in two different phosphate buffers according to the pore size sequences of the photonic gels. Since the pore size follows the sacrificed PS particle size, the color sequence of the five photonic gels was in increasing order of λ_{peak}. In Fig. 5(c), a series of reflectance spectra from the five photonic gels in two different pH buffers are shown. Each photonic gel contained VI, which exists in a deprotonated (neutral) form at high pH while it protonates below its pK_b (∼pH 4.5). Since protonated VI has a positive ionic charge, it causes swelling of hydrogel owing to Donnan potential developments, and consequently the color changed, as shown in Fig. 5(a). In addition, the five peaks shifted together since their chemical compositions were the same (i.e., HEMA/EGDM/VI). Thus, the five peaks were red-shifted at low pH (pH 2) and blue-shifted together at high pH (pH 5). By tracking λ_{peak} of the reflectance spectra with pH variation, we could obtain the pH-dependent response plots shown in Fig. 5(d). The λ_{peak} data were averaged from two independent measurements, and the corresponding error bars are included in Fig. 5(d) showing a good reproducibility of pH sensing experiment. Instead of VI in the copolymerized gel, the photonic gel sensor arrays containing an acidic monomer AA were fabricated using the same series of PS templates, and pH sensing experiments showed that an opposite color changing behavior. (See Fig. S3)

An IO photonic gel composed of HEMA/EGDM/VI fabricated by DEECA was analyzed by SEM, as shown in Fig. 6. As expected by the narrow reflectance peak and the shiny reflective color in Fig. 5, the SEM images of 20-μm-thick IO film in Fig. 6(a) and (b) clearly revealed a well-made IO structure with an FCC {111} facet parallel to the substrate surface as shown in Fig. 6(c).
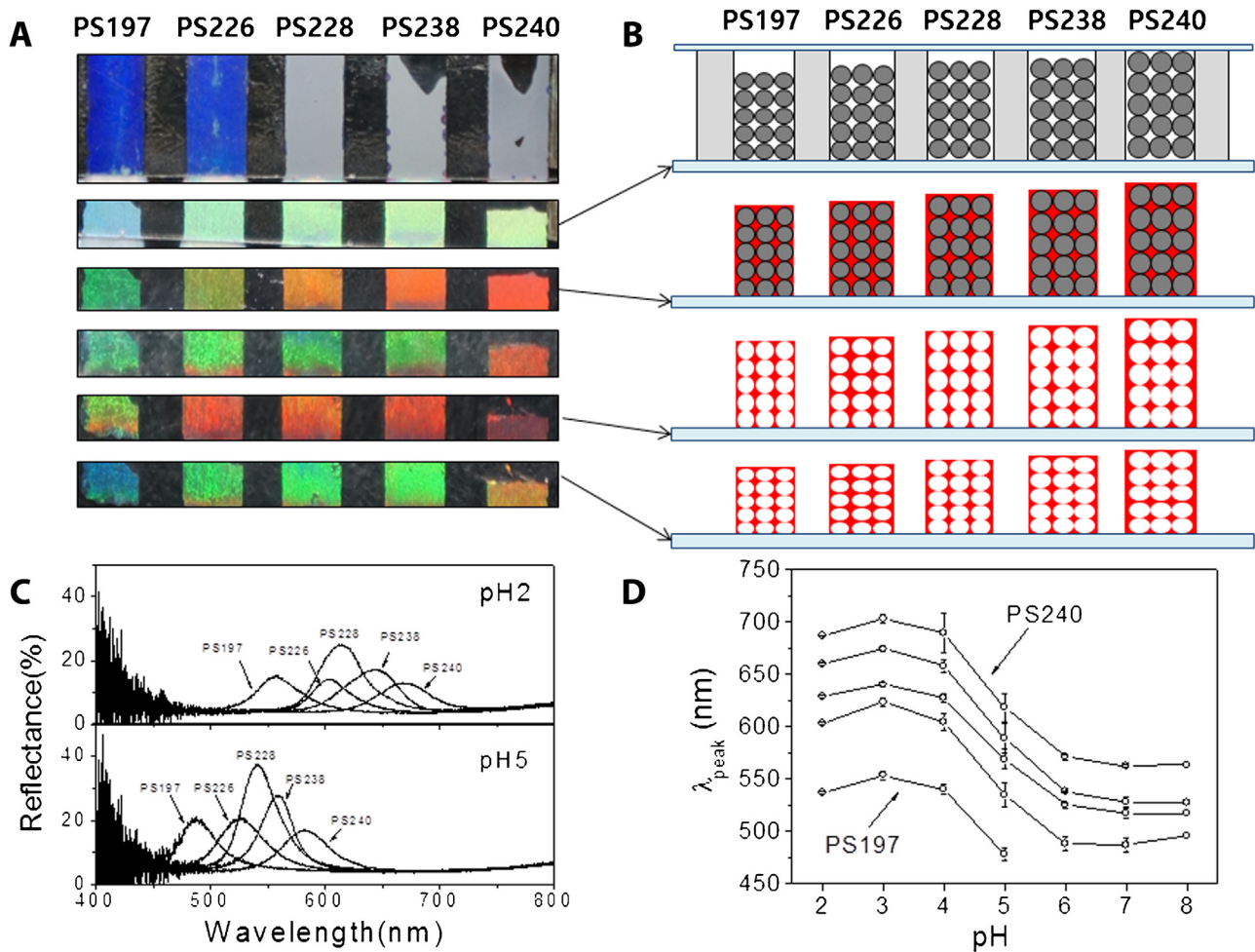
Fig. 5. On-chip integration of five photonic gel pH sensor arrays on a glass substrate using DEECA. VI-containing PHEMA IO photonic gels were fabricated using different size PS opal templates. (a) Photographs of each fabrication stage (from the top, i) after infilling the dispersions, ii) after drying, iii) after infiltrating hydrogel precursors, iv) after photopolymerization, v) after etching away PS opal templates in CHCl₃, vi) in pH2 buffer, vii) in pH5 buffer) for pH sensor arrays showing various reflective colors, (b) schematic illustrations of pH sensing photonic gel array fabrication, (c) reflectance spectra of the five pH sensor arrays in two phosphate buffers with different pH values showing red-shifted peaks at pH2 and blue-shifted peaks at pH5, respectively, and (d) plot of the average pH-dependent λ_{peak} changes of the five sensors measured from two independent pH variations. Error bar indicates the standard deviation of measurements. (For interpretation of the references to color in this figure legend, the reader is referred to the web version of this article.)
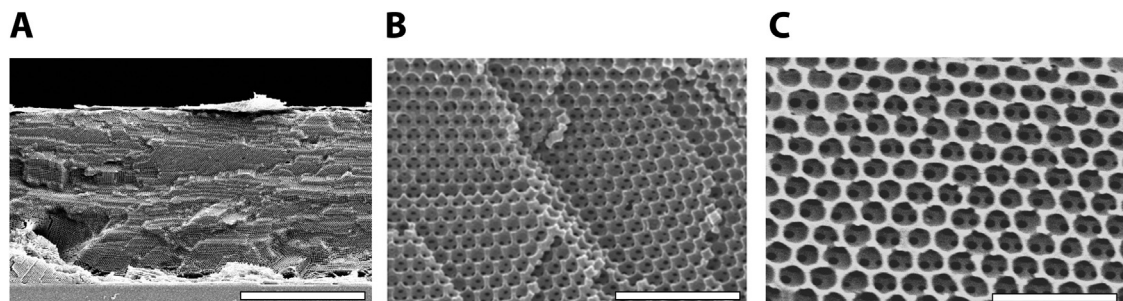

Fig. 6. SEM images of an IO photonic gel. (a) Side view, (b) enlarged side view, and (c) top view. Scale bars in a, b, and c respectively denote 10 μm, 2 μm, and 1 μm.

3.3. Photonic gel sensor array with chemically different hydrogels

In order to fabricate a photonic gel sensor array consisting of chemically different hydrogels, a linear array of three opal films of PS238 was fabricated from 10 wt% aqueous colloidal dispersion, which was subsequently infiltrated with different precursor mixtures (HEMA/EGDM/AA, HEMA/EGDM/MA, HEMA/EGDM/VI) in each respective cell, as schematically shown in Fig. 7(a). The fabrication procedures for the pH sensor arrays containing different

pH-sensing monomers were practically the same as those shown in Fig. 6(b) except for the infilling of a same-sized PS dispersion and the infilling of different monomers within the opal templates.

Because AA, MA, and VI have different pH-dependent protonation-deprotonation equilibria, changing the buffer pH resulted in different local ionic charges within each IO hydrogel, which caused distinct swelling responses and the corresponding color changes, as shown in Fig. 7(b). (See Fig. S4 for more pictures of photonic gel arrays) By tracking the peak reflectance
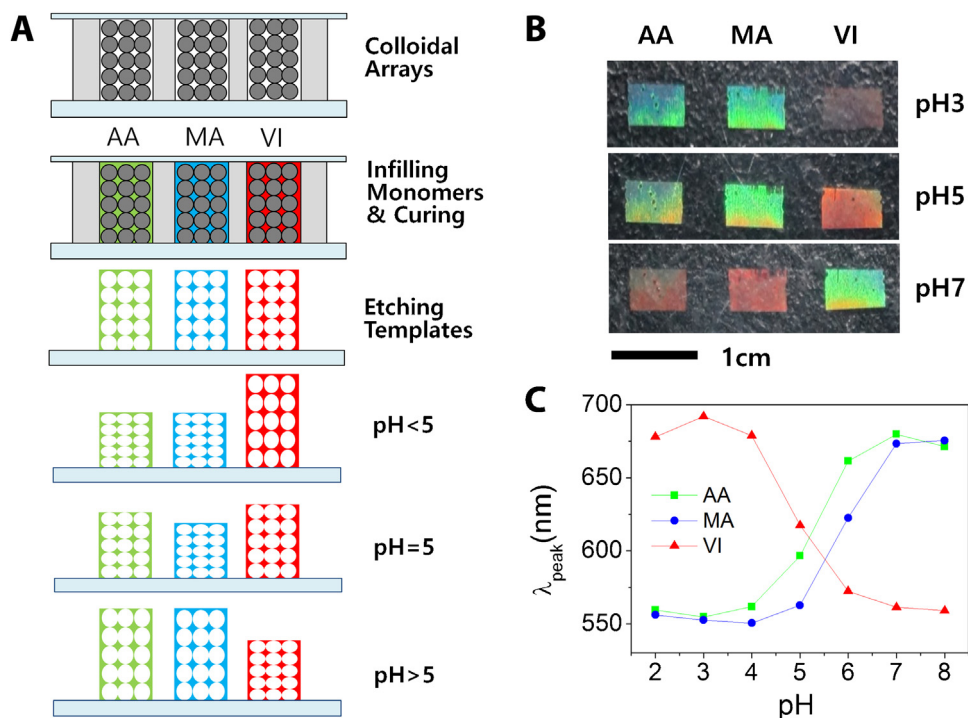
Fig. 7. Three IO photonic gel pH sensor arrays of AA, MA, and VI integrated on a single substrate. (a) Schematic illustrations of the photonic gel fabrication procedure, (b) color responses of the photonic gel pH sensors at different pH values, and (c) λ_{peak} vs. pH plots of the sensors. (For interpretation of the references to color in this figure legend, the reader is referred to the web version of this article.)
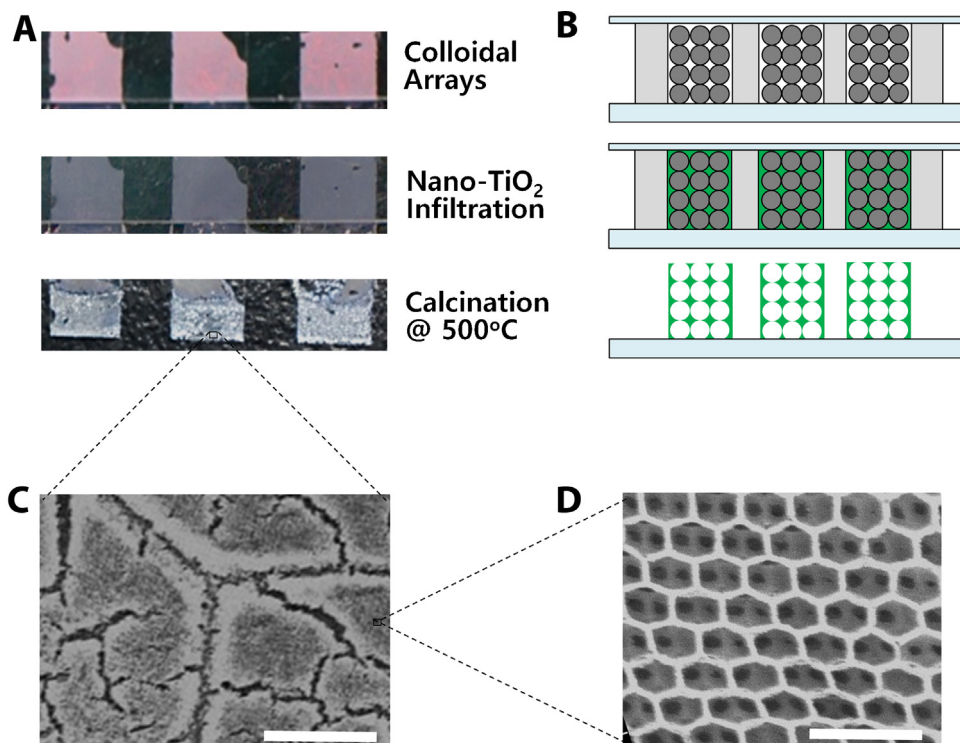

Fig. 8. TiO$_2$ nanoparticle IO films fabricated by DEECA using PS 267 for opal and acac-modified nano TiO$_2$ for IO. (a) Photographs and (b) schematic illustrations showing three stages of TiO$_2$ IO fabrication of PS opal, infiltration/drying of 10 wt% TiO$_2$ nanoparticle dispersion in ethanol, and calcinations to remove PS opal and leave TiO$_2$ IO film; (c) an SEM image of a fabricated TiO$_2$ IO film; and (d) a magnified SEM image of the TiO$_2$ IO structure. Scale bars in c and d respectively indicate 10 μm and 500 nm.

(λ_{peak}) of the reflectance spectra with pH variation, we could obtain pH-dependent response plots, as shown in Fig. 7(c). AA and MA are acidic monomers with different pKa, and thus the pH-dependent sensor responses resembled each other but showed inflection points at different pH values. The VI-containing sensor response showed a symmetric pH dependence of λ_{peak} compared to the responses of AA- or MA-containing photonic gel sensors because of its basic characteristic, in which the protonated form at low pH is positively charged to swell the photonic gel. The pH-dependent swelling/deswelling features of AA-, MA-, and VI-

containing photonic gels are demonstrated in Fig. 7(c). In S-5, two different batches of AA/VI-containing IO sensor arrays were fabricated and pH–dependent sensor responses exhibited excellent reproducibilities in color changes and reflectance changes.

3.4. TiO₂ IO film by template by DEECA opal film

DEECA-based opal film can be applied not only to the fabrication of photonic hydrogels but also to that of inorganic IO films. As shown in Fig. 8, we fabricated TiO$_2$ IO film arrays using DEECA by infiltrating a highly concentrated dispersion of organically modified TiO$_2$ nanoparticles (∼10% in ethanol) within opal arrays and by subsequent drying and thermal calcinations in a furnace. Fig. 8(a) and (b) are the photographs and the schematic illustrations of the fabrication procedure for TiO$_2$ IO film templates by DEECA-opal. In a previous report, we demonstrated that organically modified TiO$_2$ nanoparticles can be effectively infiltrated within a PS opal template by repeated spin coating of a TiO$_2$/1-butanol dispersion [27]. In this study, however, a TiO$_2$/ethanol dispersion infiltrated the opal template in the presence of a top glass plate. An excessive amount of TiO$_2$ nanoparticle dispersion that had infiltrated within the channel by capillarity was slowly dried to fill the interstitial spaces between PS μ-particles with TiO$_2$ owing to its tiny particle size (∼2 nm, see Fig. S6 for HR-TEM image), and an IO structure of TiO$_2$ after thermal calcination was confirmed by SEM analysis, as shown in Fig. 8(c) and (d). Although there were many cracks in the films due to a significant volume shrinkage during calcination of the PS/TiO$_2$ binary opal film originating from the loss of acetylacetone organic ligands, the formation of an FCC IO structure as shown in Fig. 8(d) clearly demonstrated that DEECA is again a useful method to fabricate inorganic IO films as well as organic photonic gels.

4. Conclusions

We successfully demonstrated a simple yet useful method, DEECA, for the rapid fabrication of opalline photonic crystal films without lithography. Two major driving forces—the capillarity-induced infiltration of a colloidal dispersion of PS or silica μ-particles and the evaporation-induced laminar flow and subsequent colloidal crystallization—provided high-quality opal films within 2 h. An additional advantage of DEECA is that further applications of opal templates are facilitated by capillarity-induced infiltration of precursors within interstitial spaces before the removal of the top plate. This feature was confirmed by (1) infiltration of a hydrogel precursor followed by photo-polymerization and subsequent chemical etching of the PS opal to make IO photonic gel sensor arrays and (2) infiltration of an ethanol dispersion of TiO$_2$ nanoparticles followed by drying and thermal calcinations to etch off PS to yield TiO$_2$ inorganic IO films. From the point of view of processibility, DEECA will find a variety of practical applications where on-chip integrated opal-based or IO-based photonic bandgap devices are employed in a cost-effective way.

Acknowledgement

Appendix A. Supplementary data

Supplementary data associated with this article can be found, in the online version, at http://dx.doi.org/10.1016/j.snb.2016.03.013.

References

[1] J. Shin, P.V. Braun, W. Lee, Fast response photonic crystal ph sensor based on templated photo-polymerized hydrogel inverse opal, Sens. Actuator B 150 (2010) 183–190.

[2] K. Lee, S.A. Asher, Photonic crystal chemical sensors: pH and ionic strength, J. Am. Chem. Soc. 122 (2000) 9534–9537.

[3] J.D. Debord, L.A. Lyon, Thermoresponsive photonic crystals, J. Phys. Chem. B 104 (2000) 6327–6331.

[4] Y.J. Lee, P.V. Braun, Tunable inverse opal hydrogel pH sensors, Adv. Mater. 15 (2003) 563–566.

[5] M. Xu, A.V. Goponenko, S.A. Asher, Polymerized polyHEMA photonic crystals: pH and ethanol sensor materials, J. Am. Chem. Soc. 130 (2008) 3113–3119.

[6] Y. Takeoka, M. Watanabe, Polymer gels that memorize structures of mesoscopically sized templates. Dynamic and optical nature of periodic ordered mesoporous chemical gels, Langmuir 18 (2002) 5977–5980.

[7] A.C. Arsenault, D.P. Puzzo, I. Manner, G.A. Ozin, Photonic-crystal full-colour displays, Nat. Photon. 1 (2007) 468–472.

[8] Y.G. Seo, J. Woo, H. Lee, W. Lee, Rapid fabrication of an inverse Opal TiO$_2$ photoelectrode for DSSC using a binary mixture of TiO$_2$ nanoparticles acd polymer microspheres, Adv. Funct. Mater. 21 (2011) 3094–3103.

[9] S. Guldin, S. Huttner, M. Kolle, M.E. Welland, P. Muller-Buschbaum, R.H. Friend, U. Steiner, N. Tetreault, Dye-sensitized solar cell based on a three-dimensional photonic crystal, Nano Lett. 10 (2010) 2303.

[10] S.C. Yang, D.J. Yang, J. Kim, J.M. Hong, H.G. Kim, I.D. Kim, H. Lee, Hollow TiO$_2$ hemispheres obtained by colloidal templating for application in dye-sensitized solar cells, Adv. Mater. 20 (2008) 1059–1064.

[11] Y. Nishijima, K. Ueno, S. Juodkazis, V. Mizeikis, H. Fujiwara, K. Sasaki, H. Misawa, Lasing with well-defined cavity modes in dye-infiltrated silica inverse opals, Opt. Exp. 17 (2009) 2976–2983.

[12] M.N. Shkunov, Z.V. Vardeny, M.C. DeLong, R.C. Polson, A.A. Zakhidov, R.H. Baughman, Tunable, gap-state lasing in switchable directions for opal photonic crystals, Adv. Mater. 12 (2002) 21.

[13] S.G. Han, J. Lim, J. Shin, S.M. Lee, T. Park, J. Yoon, K. Woo, H. Lee, W. Lee, Optically pumped distributed feedback dye lasing with slide-coated TiO2 inverse-opal slab as Bragg reflector, Opt. Lett. 39 (2014).

[14] A. Mihi, M. Ocana, H. Miguez, Oriented colloidal-crystal thin films by spin-coating microspheres dispersed in volatile media, Adv. Mater. 18 (2006), 2244-+.

[15] Y.A. Vlasov, X.Z. Bo, J.C. Sturm, D.J. Norris, On-chip natural assembly of silicon photonic bandgap crystals, Nature 414 (2001) 289–293.

[16] P. Jiang, J.F. Bertone, V.L. Colvin, A lost-wax approach to monodisperse colloids and their crystals, Science 291 (2001) 453.

[17] H.T. Yang, P. Jiang, Large-scale colloidal self-assembly by doctor blade coating, Langmuir 26 (2010) 13173.

[18] S.C. Gil, Y.G. Seo, S. Kim, J. Shin, W. Lee, High-speed fabrication of 3-dimensional colloidal photonic crystal films by slide coating of polymer microspheres with continuous feeding of colloidal suspension, Thin Solid Films 518 (2010) 5731–5736.

[19] J.H. Zhang, Z.Q. Sun, B. Yang, Self-assembly of photonic crystals from polymer colloids, Curr. Opin. Colloid Interface Sci. 14 (2009) 103–114.

[20] S.H. Im, M.H. Kim, O.O. Park, Thickness control of colloidal crystals with a substrate dipped at a tilted angle into a colloidal suspension, Chem. Mater. 15 (2003) 1797–1802.

[21] M.H. Kim, S.H. Im, O.O. Park, Rapid fabrication of two- and three-dimensional colloidal crystal films via confined convective assembly, Adv. Funct. Mater. 15 (2005) 1329–1335.

[22] W. Lee, S. Kim, S. Kim, J.H. Kim, H. Lee, Hierarchical opal grating films prepared by slide coating of colloidal dispersions in binary liquid media, J. Colloid Interace Sci. 440 (2015) 229–235.

[23] S.H. Park, B. Gates, Y.N. Xia, A three-dimensional photonic crystal operating in the visible region, Adv. Mater. 11 (1999) 462–466.

[24] H. Miguez, S.M. Yang, N. Tetreault, G.A. Ozin, Oriented free-standing three-dimensional silicon inverted colloidal photonic crystal microfibers, Adv. Mater. 14 (2002) 1805.

[25] S. Kim, Y.G. Seo, Y. Cho, J. Shin, S.C. Gil, W. Lee, Optimization of emulsion polymerization for submicron-sized polymer colloids towards tunable synthetic opals, Bull. Korean Chem. Soc. 31 (2010) 1891–1896.

[26] W. Stober, A. Fink, Controlled growth of monodisperse silica spheres in the micron size range, J. Colloid Interace Sci. 26 (1968) 62–69.

[27] Y.G. Seo, M.A. Kim, H. Lee, W. Lee, Solution processed thin films of non-aggregated TiO2 nanoparticles prepared by mild solvothermal treatment, Sol. Energy Mater. Sol. Cell 95 (2011) 332–335.

[28] P. Garstecki, H. Wu, TWo-dimensional colloid crystals obtained by coupling of flow and confinement, Phys. Rev. Lett. 91 (2003) 128301–128301.

Biographies

Seungjae Lee received is BS degree from Sejong University, Korea in 2015. He is currently a graduate student in Sejong University under an advice of Prof. Wonmok Lee at the Department of Chemistry. He is working on the synthesis and engineering of various nanoparticles for photonic crystal application.

Young-Lo Lee is currently an undergraduate student in Sogang University at the Department of Chemistry while he worked in Sejong University under an advice of Prof. Wonmok Lee.

Bomin Kim received her BS degree from Sejong University, Korea in 2013. She is currently a graduate student in Sejong University under an advice of Prof. Wonmok Lee at the Department of Chemistry. She is working on the fabrication of various photonic hydrogel sensors, using colloidal templating method.

Kunhyuk Kwon is currently a graduate student in Sejong University under an advice of Prof. Wonmok Lee at the Department of Chemistry. He is working on the synthesis of various organic-inorganic nanoparticles towards photonic crystal applications.

Joohyun Park received her BS degree from Sejong University, Korea in 2013. She is currently a graduate student in Sejong University under an advice of Prof. Wonmok Lee at the Department of Chemistry. She is working on the fabrication of photonic crystal sensors and displays using colloidal templating method.

Kyusung Han is a Senior Researcher of Korea Institute of Ceramic Engineering and Technology (KICET). He received BS degree at Korea University and PhD at Korea Advanced Institute of Technology. After finishing his Post-doc research in USA, he joined KICET. Dr. Han's research area covers microspic and spectroscopic characterization of various chemical species.

Hyunjung Lee is an Associate Professor of Kookmin University at the School of Advanced Materials Engineering. She received BS degree in 1995 from Pohang University of Science and Technology, MS degree in 1997 and PhD degree in 2001 from the same university. After postdoctoral periods in University of Illinois at Urbana-Champaign (UIUC) and Massachusetts Institute of Technology (MIT), Prof. Lee worked for Korea Institute of Science and Technology for 5 years. She joined the faculty at Kookmin University since 2010. Prof. Lee's research area covers the photonic crystal devices, solar cells, thermoelectric devices, and etc.

Wonmok Lee is an Associate Professor of the Department of Chemistry at Sejong University. He received his BS degree in 1995 from Pohang University of Science and Technology, MS degree in 1997 and PhD degree in 2001 from the same university. After postdoctoral periods in University of Illinois at Urbana-Champaign (UIUC) and Massachusetts Institute of Technology (MIT), Prof. Lee developed an industrial career at Samsung Advanced Institute of Technology (SAIT). He joined the faculty at Sejong University since 2007. Prof. Lee's research area covers the photonic crystal sensors, displays, and other optical devices.